Mon. Not. R. Astron. Soc. **000**, 1–?? (2009) Printed 10 December 2008 (MN LATEX style file v2.2)

# Exploring the Star Formation History of Elliptical Galaxies: Beyond Simple Stellar Populations with a New Estimator of Line Strengths

Ben Rogers[1], Ignacio Ferreras[1,2⋆], Reynier Peletier[3], Joseph Silk[4]
[1] *Department of Physics, King's College London, Strand, London WC2R 6LS*
[2] *Mullard Space Science Laboratory, Department of Space and Climate Physics, University College London, Holmbury St Mary, Dorking, Surrey RH5 6NT*
[3] *Kapteyn Astronomical Institute, University of Groningen, Postbus 800, 9700 AV Groningen, Netherlands*
[4] *Physics Department, The Denys Wilkinson Building, Keble Road, Oxford, OX1 3RH*



Submitted for publication in MNRAS, 10 Dec, 2008

**ABSTRACT**
We study the stellar populations of a sample of 14 elliptical galaxies in the Virgo cluster. Using spectra with high signal-to-noise ratio (S/N $\gtrsim 100$Å $^{-1}$) we propose an alternative approach to the standard side-band method to measure equivalent widths (EWs). Our *Boosted Median Continuum* is shown to map the EWs more robustly than the side-band method, minimising the effect from neighbouring absorption lines and reducing the uncertainty at a given signal to noise ratio. Our newly defined line strengths are more sucessful at disentangling the age-metallicity degeneracy. We concentrate on Balmer lines (H$\beta$,H$\gamma$,H$\delta$), the G band and the 4000Å break as age-sensitive indicators, and on the combination [MgFe] as the main metallicity indicator. We go beyond the standard comparison of the observations with simple stellar populations (SSP) and consider four different models to describe the star formation histories, either with a continuous star formation rate or with a mixture of two different SSPs. These models improve the estimates of the more physically meaningful mass-weighted ages. Composite models are found to give more consistent fits among individual line strengths and agree with an independent estimate using the spectral energy distribution. A combination of age and metallicity-sensitive spectral features allows us to constrain the average age and metallicity. Our age and metallicity estimates correlate well with stellar mass or velocity dispersion, with a significant threshold around $5 \times 10^{10} M_{\odot}$ above which galaxies are uniformly old and metal rich. This threshold is reminiscent of the one found by Kauffmann et al. in the general population of SDSS galaxies at a stellar mass $3 \times 10^{10} M_{\odot}$. In a more speculative way, our models suggest that it is formation *epoch* and not formation timescale what drives the Mass-Age relationship of elliptical galaxies.

**Key words:** galaxies: elliptical and lenticular, cD – galaxies: evolution – galaxies: formation – galaxies: stellar content.

## 1 INTRODUCTION

Unveiling the star formation histories of elliptical galaxies is key to our understanding of galaxy formation. Being able to resolve their seemingly homogenous distribution is hampered by the fact that their light is dominated by old, i.e. low-mass stars, which do not evolve significantly even over cosmological times. Furthermore, the presence of small amounts of young stars as recently discovered in NUV studies (Ferreras & Silk 2000; Yi et al. 2005; Kaviraj et al. 2007a) reveals a complex history of star formation that requires proper estimates of mass-weighted ages, in contrast with the luminosity-weighted ages that simple stellar populations (SSPs) can only achieve. The majority of papers dealing with age estimates of the stellar populations of elliptical galaxies rely on such SSPs (see e.g. Kuntschner & Davies 1998; Trager et al. 2000; Thomas et al. 2005), and it is only recently that special emphasis has been made on the need to go beyond simple populations (Ferreras & Yi 2004; Serra & Trager 2007; Idiart et al. 2007)

Dating the (old) stellar populations of elliptical galaxies has ben fraught with difficulties, the most prominent being the age-metallicity degeneracy, whereby the photo-spectroscopic properties of a galaxy of a given age and metallicity can be replicated by a younger or older galaxy at a suitably higher or lower metallicity, respectively. To some extent, this problem has been overcome by the measurement of pairs of absorption line indices (Worthey 1994), one whose change in equivalent width (EW) is dominated by the average metallicity of the population and the other dominated by the average age of the population. Typical metal-sensitive line strengths are the Mg feature at 5170Å , the iron lines around 5300Å, or a combination such as [MgFe] González (1993). Balmer lines

⋆ E-mail: ferreras@star.ucl.ac.uk

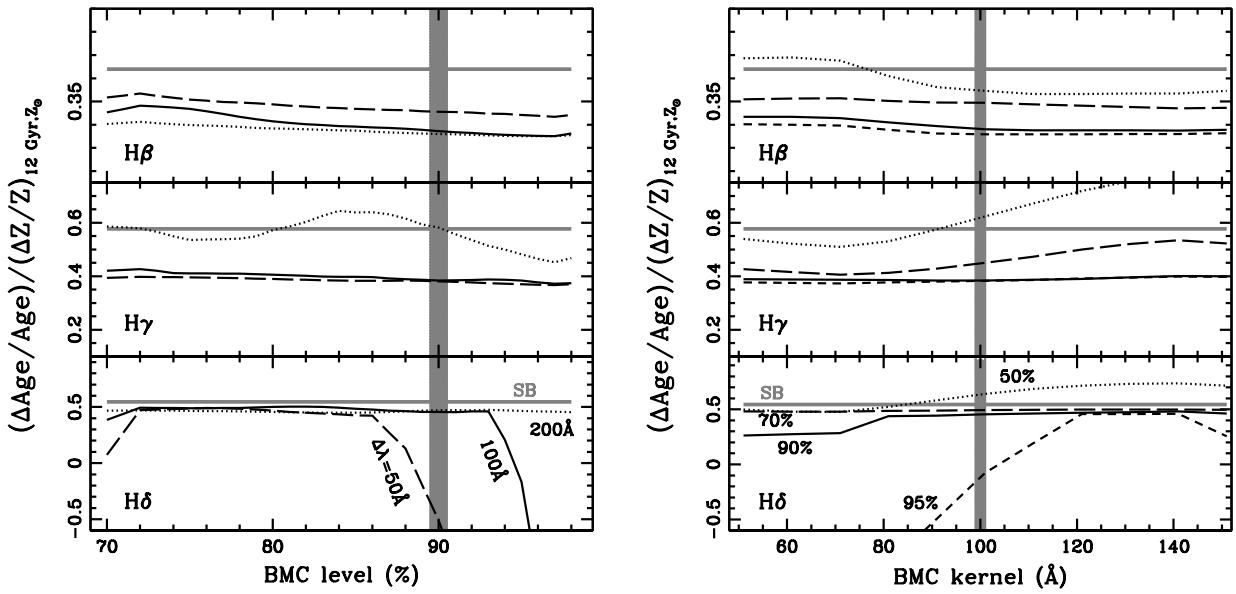


**Figure 1.** Dependence of the age-metallicity gradient – ($\Delta$ Age/Age)(/$\Delta$ Z/Z) – on the choice of BMC parameters, namely the level at which the 'boosted median' is taken (*left*) or the size of the kernel (*right*). On the left panel a number of kernel sizes is shown as labelled: $\Delta\lambda$=50Å (dashed); 100Å (solid) and 200Å (dotted). On the right panel a number of confidence levels are considered: 50% (dotted); 70% (long dashed); 90% (solid) and 95% (short dashed). The grey horizontal line in both panels is the estimate from the standard side-band method (SB), and the grey vertical shaded area marks our choice of 'boosted median' parameters.

are more age-sensitive and are often combined with those lines to break the degeneracy. However, measurements of EWs of Balmer lines can be affected by the age-metallicity degeneracy because of the presence of nearby absorption lines. Such is the case of H$\gamma$, with the prominent G band at 4300Å or the CN bands in the vicinity of the H$\delta$ line. This paper is partly motivated by the need to define a method to estimate EWs that minimise the sensitivity of metallicity on Balmer lines by a proper estimate of the continuum.

Even at relatively younger ages (a few Gyrs) where such uncertainties are reduced, considerable degeneracies still remain. The confirmation of recent star formation (RSF) occuring in early type galaxies (Yi et al. 2005; Kaviraj et al. 2007a) has raised the problem that the existence of a young population can considerably affect the parameters derived through SSP analysis. Trager et al. (2000) and later Serra & Trager (2007) showed that even relatively small fractions ($\sim$1%) of young stars can can distort age and metallicity estimates and in moderate cases ($\sim$10%) completely overshadow the older population. In addition, the age and mass fraction of any younger sub-population will also be degenerate, with larger mass fraction of relatively older sub populations having the same effect as smaller fractions of younger ones.

Schiavon et al. (2004) noticed that using different Balmer lines (H$\beta$, H$\gamma$ and H$\delta$) to estimate the age gives slightly different results, which was suggested to show that the galaxy had undergone recent star formation. Contrary to this, Thomas et al. (2004) find that H$\gamma$ and H$\delta$ equivalent widths are more affected by a non-solar $\alpha$/Fe ratio on higher order Balmer lines. This effect is due to the increase of metal lines at bluer wavelengths, thereby distorting the continuum as measured by a side-band method. This was expanded by Serra & Trager (2007) who remodelled synthetic 2 burst models using H$\beta$ and H$\gamma_A$ and achieved a result consistent with both papers, concluding that the three Balmer line estimates could possibly reveal underlying younger populations through their disagreement.

Moving forward with such analysis – beyond simple populations and luminosity weighted parameters – requires improvements on both the H$\gamma$ and H$\delta$ measurements. Balmer line equivalent widths suffer from the effects of the metallicity due to the presence of such lines in their surrounding wavelengths, used to determine the continuum (Worthey & Ottaviani 1997; Thomas et al. 2004; Prochaska et al. 2007). Although considerable work has already been done in this area (see e.g. Rose et al. 1994; Jones & Worthey 1995; Vazdekis & Arimoto 1999; Yamada et al. 2006), we test a completely different approach.

In this paper we present a comprehensive analysis of the stellar populations of 14 Virgo cluster ellipticals using several models to describe the star formation history, exploring the discrepancies found between simple and composite stellar populations. In an attempt to combat the problems discussed above, we introduce a new method for the measurement of equivalent widths using a high percentile running median to describe the continuum. The properties of this new method are exploited by using various age- and metallicity-sensitive spectral features.

## 2 THE SAMPLE

We use a sample of 14 elliptical galaxies in the Virgo cluster, for which moderate resolution spectroscopy is available at high signal-to-noise ratio (S/N $\gtrsim$ 100 Å$^{-1}$, Yamada et al. 2006, 2008). Eight galaxies were observed with FOCAS at the 8m Subaru telescope; the other six were observed with ISIS at the 4.2m William Herschel Telescope (WHT). Observations from Subaru span the spectral range $\lambda \simeq 3800 - 5800$Å , whereas the spectra taken at the WHT span a narrower window, namely $\lambda \simeq 4000 - 5500$Å . The

**Table 1.** Equivalent Widths of Virgo Elliptical galaxies using a 90% Boosted Median Continuum (see text for details). All values given in Å , with the $1\sigma$ uncertainties in brackets below each measurement.

| Galaxy | $\sigma^1$ | H$\beta_{20}$ | H$\gamma_{20}$ | H$\delta_{20}$ | Mgb$_{20}$ | Fe5270$_{20}$ | Fe5335$_{20}$ | G4300$_{20}$ | D4000 | [MgFe]$_{20}$ |
|---|---|---|---|---|---|---|---|---|---|---|
| NGC 4239 | 63 | 2.993 | 2.097 | 2.356 | 2.972 | 2.864 | 1.673 | 6.130 | 1.441 | 2.596 |
| | | (0.051) | (0.064) | (0.056) | (0.044) | (0.046) | (0.060) | (0.046) | (0.006) | (0.032) |
| NGC 4339 | 114 | 2.666 | 1.488 | 1.442 | 3.807 | 3.163 | 1.772 | 6.642 | 1.560 | 3.065 |
| | | (0.047) | (0.054) | (0.082) | (0.045) | (0.037) | (0.050) | (0.042) | (0.005) | (0.024) |
| NGC 4365 | 261 | 2.191 | 0.732 | 1.195 | 3.819 | 2.971 | 1.615 | 6.289 | — | 2.959 |
| | | (0.026) | (0.042) | (0.070) | (0.023) | (0.028) | (0.031) | (0.021) | (—) | (0.015) |
| NGC 4387 | 112 | 2.431 | 1.698 | 1.974 | 3.614 | 3.237 | 1.703 | 7.317 | — | 2.988 |
| | | (0.044) | (0.066) | (0.068) | (0.039) | (0.057) | (0.061) | (0.050) | (—) | (0.024) |
| NGC 4458 | 106 | 2.464 | 1.622 | 1.676 | 3.520 | 2.719 | 1.670 | 6.570 | 1.504 | 2.779 |
| | | (0.039) | (0.053) | (0.055) | (0.037) | (0.042) | (0.047) | (0.041) | (0.006) | (0.025) |
| NGC 4464 | 121 | 2.302 | 1.547 | 1.523 | 3.648 | 2.913 | 1.521 | 6.813 | — | 2.844 |
| | | (0.038) | (0.053) | (0.070) | (0.035) | (0.034) | (0.036) | (0.037) | (—) | (0.023) |
| NGC 4467 | 83 | 2.605 | 1.797 | 1.875 | 3.839 | 3.209 | 1.747 | 6.760 | 1.458 | 3.085 |
| | | (0.050) | (0.063) | (0.065) | (0.044) | (0.052) | (0.056) | (0.049) | (0.005) | (0.026) |
| NGC 4472 | 303 | 2.225 | 0.793 | 1.149 | 3.650 | 2.719 | 1.535 | 5.742 | 1.525 | 2.787 |
| | | (0.031) | (0.069) | (0.081) | (0.039) | (0.039) | (0.042) | (0.027) | (0.005) | (0.021) |
| NGC 4473 | 193 | 2.410 | 1.233 | 1.592 | 3.990 | 3.212 | 1.808 | 6.918 | — | 3.164 |
| | | (0.028) | (0.044) | (0.060) | (0.026) | (0.023) | (0.041) | (0.020) | (—) | (0.021) |
| NGC 4478 | 143 | 2.627 | 1.653 | 1.855 | 3.719 | 3.378 | 1.838 | 6.764 | — | 3.114 |
| | | (0.042) | (0.051) | (0.069) | (0.036) | (0.039) | (0.040) | (0.039) | (—) | (0.023) |
| NGC 4489 | 62 | 3.204 | 2.084 | 2.328 | 3.217 | 3.248 | 1.903 | 6.455 | 1.520 | 2.878 |
| | | (0.047) | (0.054) | (0.075) | (0.046) | (0.048) | (0.045) | (0.050) | (0.005) | (0.028) |
| NGC 4551 | 113 | 2.663 | 1.717 | 1.736 | 3.907 | 3.416 | 2.027 | 6.828 | 1.531 | 3.261 |
| | | (0.046) | (0.058) | (0.056) | (0.034) | (0.038) | (0.044) | (0.036) | (0.005) | (0.024) |
| NGC 4621 | 230 | 2.284 | 0.964 | 1.312 | 4.072 | 3.014 | 1.678 | 6.250 | — | 3.091 |
| | | (0.016) | (0.024) | (0.040) | (0.012) | (0.017) | (0.018) | (0.011) | (—) | (0.009) |
| NGC 4697 | 181 | 2.397 | 1.289 | 1.661 | 3.806 | 3.198 | 1.832 | 6.603 | 1.524 | 3.094 |
| | | (0.029) | (0.037) | (0.071) | (0.027) | (0.026) | (0.033) | (0.021) | (0.004) | (0.017) |

[1] Velocity dispersions given in km/s, from McElroy (1995).

resolution of both data sets is similar: 2Å (Subaru) and 2.4Å(WHT) FWHM. We refer the interested reader to Yamada et al. (2006) for details about the data reduction process. We compare those spectra with composites of the R$\sim$ 2000 synthetic models of Bruzual & Charlot (2003). We resampled the observed spectra from the original 0.3Å to 1Å per pixel, performing an average of the spectra over a 1.5Å window, in order to have a sampling more consistent with the actual resolution.

Notice that Morelli et al. (2004) reported that NGC 4458 has a decoupled core, however their analysis indicated that the stellar population properties between the core and the main part of the galaxy were indistinguishable so it is not expected that this should change any results within the paper.

In this paper we use two alternative sets of information, either the full spectral energy distribution or targeted absorption lines. For the former, we consider a spectral window around the 4000Å break, which is a strong age indicator (albeit with a significant degeneracy in metallicity, especially for evolved stellar populations). In order to minimise the effect of an error in the flux calibration, we do not choose the full spectral range of the spectra, restricting the analysis to 3800–4500Å for the Subaru spectra, and 4000–4500Å for the WHT spectra.

The second method focuses on a reduced number of spectral lines. Following the traditional approach (see e.g. Kuntschner & Davies 1998; Trager et al. 2000; Thomas et al. 2005; Sánchez-Blázquez et al. 2006), we use a set of age-sensitive and metallicity-sensitive lines from the Lick system (Worthey et al. 1994) and its extensions (Worthey & Ottaviani 1997). In the next section we describe in detail the indices targeted by our analysis and describe a new algorithm that improves on the "standard" method to determine the continuum in galaxy spectra.

## 3 MEASURING EQUIVALENT WIDTHS

We focus on a reduced set of absorption lines originally defined in the Lick/IDS system (Worthey et al. 1994) and extensions thereof (Worthey & Ottaviani 1997). As age-sensitive lines we use the Balmer lines H$\beta$, H$\gamma$, H$\delta$, the G-band G4300 and the 4000Å break (D4000). As metal-sensitive tracer we use the standard definition of [MgFe] (González 1993), which is a reliable tracer of overall metallicity, with a very mild dependence on [$\alpha$/Fe] abundance ratio (Thomas et al. 2003).

The standard method to determine the equivalent widths of galaxy spectra relies on the definition of a blue and a red side-band to determine the continuum. A linear fit to the average flux in the blue and red side-bands is used to track the continuum in the line (see e.g. Trager et al. 2000). This method, although easy to implement, has an important drawback as neighbouring lines can make a significant contribution to the flux in the blue and red passbands, introducing unwanted age/metallicity effects. For instance, the H$\gamma$ index (Worthey & Ottaviani 1997) is defined with the blue side-band located close to the prominent G-band, around 4300Å . This definition causes non-physical negative values of the H$\gamma$ line in *absorption*, as the depression caused by the G-band makes the flux in the $H\gamma$ line (wrongly) apprear in *emission*. This has not prevented the community from using this line as a sensitive age tracer, as long as

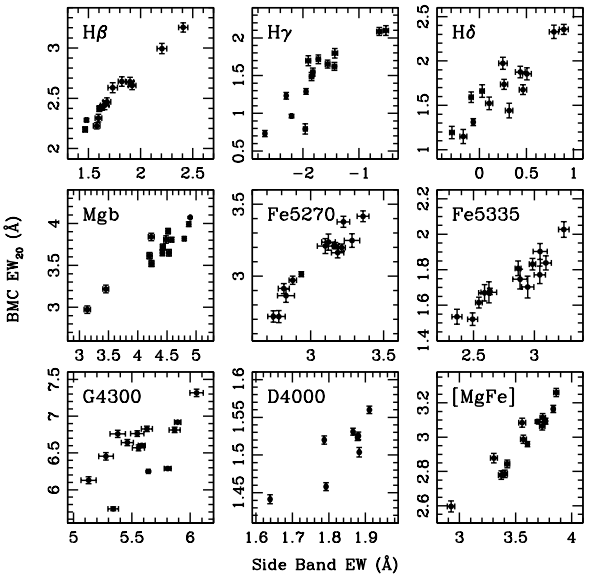


**Figure 2.** Comparison between the results of the side-band method (SB) and our proposed 'Boosted Median Continuum' (BMC) for H$\beta$, H$\gamma_F$, H$\delta_F$, Mgb, Fe5270, Fe5335, G4300, D4000 and [MgFe]. Error bars are shown at the 1$\sigma$ level. Notice only 8 galaxies (observed with Subaru) have a measurement of the 4000Å break. For the remaining six galaxies our data does not extend bluer than 4000Å.

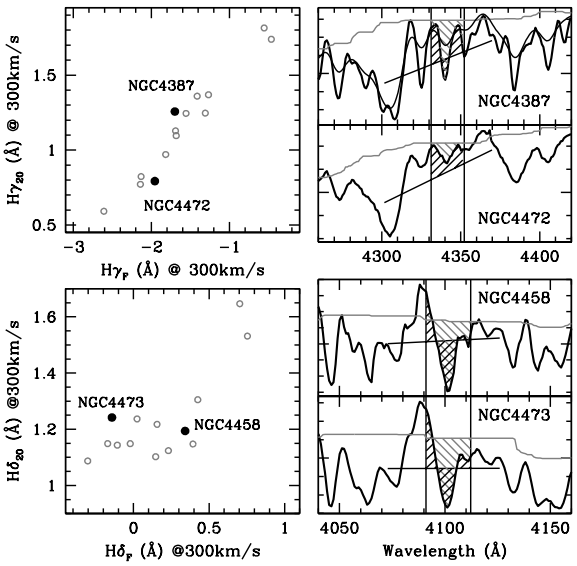


**Figure 3.** Comparison of the H$\gamma_F$ and H$\delta_F$ equivalent width measured with the side-band (SB) and the Boosted Median method (BMC). In order to eliminate the dependence of the EWs on velocity dispersion, we have done the measurements on spectra broadened to the maximum velocity dispersion of the sample ($\sim$ 300 km/s). As an example, the smoothed SED of NGC4387 is shown as a thin black line in the upper-right panel. We highlight in black some of the galaxies with a significant difference between both methods. On the right, the spectral energy distribution of the selected galaxies is shown (black line), focused on the region of interest, with the slanted line representing the continuum defined by the SB method, and the grey line showing the BMC pseudo-continuum. The hatched black (grey) regions illustrate the EW measured according to the side-band (BMC) method.

models and data are treated in the same way. Vazdekis & Arimoto (1999) defined new measurements of this line in order to reduce the metallicity degeneracy mainly introduced by the choice of the side bands. They avoid this by selecting specific regions less affected by the metal absorption lines.

H$\delta$ is another Balmer line which has been recently considered to be affected by neighbouring metal lines – most notably the CN molecular bands – which reduce the age sensitivity of the index (Prochaska et al. 2007).

In this paper we present an alternative method to determine the equivalent widths. Our method does not rely on the definition of blue and red side-bands and minimizes the contamination from neighbouring lines. This method is simple to apply and we propose it for future studies of stellar populations in galaxies[1].

### 3.1 The Boosted Median Continuum (BMC)

Our measure of equivalent width follows the standard procedure comparing observed flux in the line and the corresponding "interpolated" continuum in the same wavelength range. For an equivalent width measured in Å:

$$EW = \int_{\lambda_1}^{\lambda_2} \Big[1 - \frac{\Phi(\lambda)}{\Phi_C(\lambda)}\Big] d\lambda, \quad (1)$$

where $\lambda_1$ and $\lambda_2$ define the wavelength range of the line, $\Phi(\lambda)$ is the observed flux, and $\Phi_C(\lambda)$ is the flux from the continuum. Rather than defining the continuum as a linear fit between a blue and a red side-band, we propose the "boosted median" of the flux, defined at each wavelength as the 90th percentile of the flux values within a 100Å window.

This method is defined by two parameters, namely the choice of percentile (90% in our case) and the size of the kernel ($\Delta\lambda$ =100Å). The kernel size needs to be large enough to avoid the small scale variations of the spectra, but small enough to avoid distortions from large scale structure of the spectra such as the breaks at 4000Å and 4300Å, or flux calibration errors. The choice of percentile also suffers a similar balancing act, since it should be high enough to select the true continuum but at a value that would avoid it becoming dominated by noise. In order to determine the optimal choice, a range of values for these two parameters was studied on a number of simple stellar populations taken from the models of Bruzual & Charlot (2003) including the effect of velocity dispersion and noise. Out of the simulations, we adopted the 90th percentile of the flux within a 100Å window. However, this choice is not critical, given the robustness of the method in which the continuum is selected (i.e. a median). The advantage of averaging over a large enough wavelength range is that the effect of strong metallic lines in the vicinity of the index is limited. Furthermore, this pseudo-continuum is found to be less susceptible to noise (see below).

Figure 1 motivates our choice of parameters. We show the age-metallicity sensitivity – ($\Delta$Age/Age)/($\Delta$Z/Z) – for simple stellar populations measured at 12 Gyr and solar metallicity. We do not follow the same definition as in Worthey (1994). Instead, we change

[1] A C-programme that computes EWs using our proposed BMC method from an ASCII version of an SED can be obtained from us (`ferreras@star.ucl.ac.uk`).

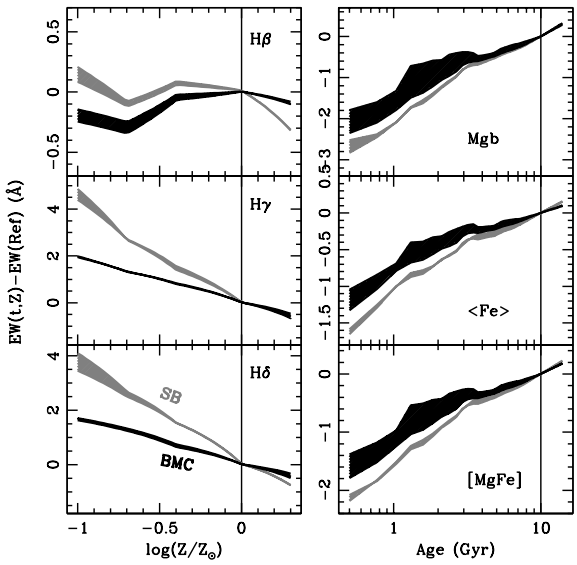


**Figure 4.** Dependence of Balmer lines on metallicity (*left*) and "metal" lines on age (*right*). The standard side-band method (SB; grey) and our proposed Boosted Median Continuum (BMC; black) are shown for a range of metallicities and ages as shown. On the left, the shaded areas correspond to an age range $[6, 12]$ Gyr. On the right, the shaded areas span a range of metallicities: $-0.3 < \log Z/Z_{\odot} < +0.3$. The vertical axis is the difference between the equivalent width of the line for a given metallicity (left) or age (right) and the value at a reference point given by the vertical line (i.e. solar metallicity on the left and 10 Gyr on the right).

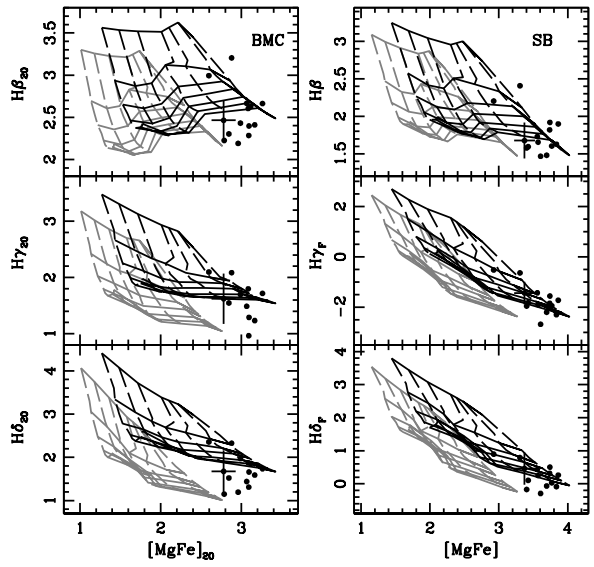


**Figure 5.** Comparison of grids of SSP models using the standard side-band method (SB, *right*) and our proposed Boosted Median Continuum (BMC, *left*). A systematic error bar is included in each panel (the observational error bars are much smaller). We show the grids for two different velocity dispersions 100km/s (black) and 300km/s (grey). The solid lines connect the SSPs with ages (from top to bottom) 2 to 14 Gyr in steps of 2 Gyr. The dashed lines connect the SSPs with metallicities (from left to right) [m/H]=−1 to +0.2 in steps of 0.2 dex.

the age from the reference value by 2 Gyr and find the metallicity change required from a reference SSP with 12 Gyr and solar metallicity that gives the same variation in the EW. The grey horizontal bar is the value determined from the standard side-band method. Smaller values of the gradient imply a better disentanglement of the age-metallicity degeneracy. In the left (right) panels the horizontal axis explores a range of confidence levels (kernel sizes). The lines correspond to various choices of kernel size (left) and confidence level (right) as labelled. H$\beta$ (*top*) behaves quite robustly with respect to the choice of BMC parameters. H$\gamma$ (*middle*) shows that the presence of large scale features such as the break found around the G band at 4300Å can affect the estimate if a large kernel size is chosen (200Å, dotted line, *left*). Finally, H$\delta$ (*bottom*) shows that too small a kernel size ($\Delta\lambda$ =50Å, dashed line, *left*) or too high a confidence level (95%, short dashed line, *right*) can affect the estimate. In this case the effect is caused by nearby features that will contaminate the estimate of the pseudo-continuum. Our choice of 100Å kernel size and 90% level is thereby justified by the need to avoid both short and long-scale features in the SEDs. Furthermore, lower confidence levels should be avoided as they will give flux values closer to an average that will not reflect the true continuum given the presence of numerous absorption lines. Too high values of the level will make the measurement more prone to higher uncertainties at low signal-to-noise ratios. Monte Carlo simulations of noise show that for our choice of BMC parameters the errors for the BMC are as small if not smaller than those from the standard side-band method.

Hence, the method for generating the BMC is fairly simple. At every wavelength the 90th percentile from all flux measurements within 50Å on either side is assigned as the continuum at that wavelength. With the continuum thus defined, for each line strength we only have to define the central wavelength and the spectral window over which the line is measured. Given that our method maps quite robustly the underlying continuum, we decided to fix a 20Å width for all line strengths considered in this paper – hereafter, our BMC-based equivalent widths are labelled with a 20 subindex.

This is motivated by the fact that for some definitions of the line strengths, any 'contaminating' lines falling within the central bandpass can have a stronger effect on the BMC method compared to the standard side-band method. A clear example is found in the $H\beta$ line, where the effect of FeI( 4871Å) which sits on the shoulder of the Balmer line within the standard definition of the central passband (width 28.75Å ) clearly distorts the measurement of the equivalent width. This is slightly 'compensated' in the side-band method through the presence in the blue side-band of another significant Fe line at 4891Å. This is clearly not the case for the BMC method, in which the pseudo-continuum is effectively independent of the values of both Fe absorption lines. Hence, in the BMC method it is desirable to choose a central passband which only targets the line of interest. However, the method is versatile enough to define wider central bandpasses.

Thus, to avoid this problem we define a central passband wavelength as narrow as possible within the usual spectral resolutions targeted in unresolved stellar populations. We follow the 'F' type passbands used for the Balmer indices (Worthey & Ottaviani 1997), defining a 20Å window centered on the line of interest[2]. In the case of the metal lines – which in most cases are clusters of lines – the major feature is chosen as the center of the new index.

[2] Our BMC-based EWS are labelled with a '20' subindex, e.g. H$\beta_{20}$

**Table 2.** Range of parameters explored in this paper (see text for a description of each model).

| Model/Param | MIN | MAX | Comments |
|---|---|---|---|
| SSP | | | 2 params |
| Age | 1 | 13 | Gyr |
| $\log(Z/Z_{\odot})$ | -1.5 | +0.3 | Metallicity |
| EXP | | | 3 params |
| $\log \tau$ (Gyr) | -1 | +0.9 | Exp. Timescale |
| $z_F$ | 1 | 5 | Formation epoch |
| $\log(Z/Z_{\odot})$ | -1.5 | +0.3 | Metallicity |
| 2BST | | | 4 params |
| $t_O$ | 5 | 13 | Old (Gyr) |
| $t_Y$ | 0.1 | 3 | Young (Gyr) |
| $f_Y$ | 0.0 | 0.5 | Mass fraction |
| $\log(Z/Z_{\odot})$ | -1.5 | +0.3 | Metallicity |
| CXP | | | 3 params |
| $\log \tau_1$ (Gyr) | -1 | +0.9 | SF Timescale |
| $\log \tau_2$ (Gyr) | -1 | +0.9 | Enrichment Timescale |
| $z_F$ | 1 | 5 | Formation epoch |

In the case of $\mathrm{Mgb}_{20}$, this is centered between the MgI doublet at 5167/5172Å. $\mathrm{Fe5270}_{20}$ is defined by the FeI line at 5270Å and $\mathrm{Fe5335}_{20}$ uses the FeI line at 5328Å. The central passband of the G-band is 4300Å. Such a simple approach is nevertheless very versatile in its definition of any line strength. The new $D4000$ break feature uses the definition given by Balogh et al. (1999), with the difference that it is the ratio of the continuum flux obtained by the BMC method within those wavelengths that is used here.

Table 1 shows the (BMC-measured) equivalent widths of the Virgo elliptical galaxies targeted in this paper. The measurements are obtained directly from the observed spectra, presented in Yamada et al. (2006) and have not been corrected with respect to velocity dispersion. Analogously to the standard method, one could either correct the observed EWs for the effect of velocity dispersion, or use the observed EWs in the modelling. For the latter, one must then measure the model EWs on spectra with the same resolution and velocity dispersion as the targeted galaxy. We follow this approach in the paper. The numbers in brackets correspond to the 1-$\sigma$ uncertainty, obtained from a Monte Carlo simulation that generates 500 realizations of each SED, adding noise corresponding to the SNR of the observations. Notice that 6 of the galaxies do not have a measured D4000 as they were observed over a spectral range that does not include the blue passband used in the definition of D4000.

### 3.2 Comparison with the side-band method

While the BMC method is different in its approach, we should expect the measurements to correlate with the values of the side-band method and only in the cases where neighbour lines distort the pseudo-continuum would we expect to see a divergence. A comparison is shown in figure2. One can see that for Mgb, Fe5270 and Fe5335, there is a clear linear relationship between both methods. If we now look at the H$\beta$, H$\gamma_F$ and H$\delta_F$ indices, we notice a wider spread in the correlation. In the cases of H$\beta$ and H$\gamma_F$ – and to some extend Fe5270 – there appears to be a 'saturation' effect of the traditional side-band method at the lower end. Those galaxies have similar EWs of H$\beta$ and H$\gamma_F$ in the traditional side-band method, whereas the BMC measurement gives a wider range of values of the EW. Figure 3 compares the H$\gamma_F$ and the H$\delta_F$ lines from both methods. In order to eliminate the dependence of the EWs on velocity dispersion, we have done the measurements on spectra broadened to the maximum velocity dispersion of the sample ($\sim$ 300 km/s for NGC 4472). The left panels show the full sample as open grey circles, but we focus on two galaxies in each case (solid dots). Those galaxies are chosen because they have a similar value using one method, and a significantly different value using the other method. The spectral regions targeted in those galaxies is shown in the rightmost panels, including the observed SED (in black), the BMC pseudo-continuum in grey, and a straight line following the standard side-band definition of the continuum. The vertical line shows the position of the Balmer line for each case, and the hatched regions in black (grey) illustrates the EW according to the side-band (BMC) method.

In the top panels (H$\gamma_F$) NGC4387 and NGC4472 have a similar EW using the side-band method, whereas they differ by about 0.5Å in the BMC method. The SEDs reveal that these two galaxies have very different Balmer absorption, but the side-band method is "tricked" when comparing the flux with the continuum (straight line). Both have similar areas above the continuum, giving a similar (negative) equivalent width. Similarly, in the bottom panels, we focus on NGC4473 and NGC4458. These galaxies give a similar BMC-based EW but a very different side-band measurement. The SEDs on the rightmost panels show that the lines are similar, but the neighbouring features add more light within the central passband in NGC4473, giving a more negative value of the EW. Furthermore, the side-bands are more affected in NGC4473 by heavy CN absorption, reducing the continuum as can be seen by a comparison of the pseudo-continuum of the side-band method (slanted black line) with the BMC method (grey line). Notice the dent in the estimate of the BMC continuum of NGC4473 around 4150Å. This is caused by CN features, which are significantly stronger in NGC4473 ($\mathrm{CN}_1$=0.138Å) than in NGC4458 ($\mathrm{CN}_1$=0.074, from Yamada et al. 2006).

Therefore, figure 3 shows that our proposed method is more resilient to the effects of neighbouring absorption features. To further illustrate this point, figure 4 compares the age-metallicity degeneracy of typical Balmer (*left*) and metal lines (*right*) measured

**Table 3.** Ages and metallicities of Virgo elliptical galaxies according to the four models used in this paper. Error bars quoted at the 90% confidence level.

| Galaxy | SSP | | | EXP | | | 2BST | | | CXP | | |
|---|---|---|---|---|---|---|---|---|---|---|---|---|
| NGC | Age(Gyr) | log(Z/Z$_\odot$) | $\chi^2_r$ | Age(Gyr) | log(Z/Z$_\odot$) | $\chi^2_r$ | Age(Gyr) | log(Z/Z$_\odot$) | $\chi^2_r$ | Age(Gyr) | log(Z/Z$_\odot$) | $\chi^2_r$ |
| 4239 | $5.2^{+1.5}_{-1.3}$ | $-0.20^{+0.11}_{-0.10}$ | 0.12 | $5.9^{+1.9}_{-1.5}$ | $-0.22^{+0.12}_{-0.09}$ | 0.09 | $6.8^{+2.8}_{-2.0}$ | $-0.21^{+0.13}_{-0.10}$ | 0.15 | $6.0^{+2.1}_{-1.5}$ | $-0.03^{+0.09}_{-0.11}$ | 0.10 |
| 4339 | $8.1^{+2.8}_{-2.4}$ | $+0.08^{+0.11}_{-0.15}$ | 0.36 | $8.2^{+2.1}_{-2.3}$ | $+0.09^{+0.11}_{-0.13}$ | 0.40 | $8.3^{+2.6}_{-2.6}$ | $+0.16^{+0.10}_{-0.15}$ | 0.49 | $9.2^{+1.6}_{-1.7}$ | $+0.20^{+0.05}_{-0.06}$ | 0.33 |
| 4365 | $11.7^{+0.9}_{-1.3}$ | $+0.23^{+0.05}_{-0.05}$ | 0.04 | $11.0^{+0.7}_{-1.0}$ | $+0.24^{+0.04}_{-0.04}$ | 0.06 | $11.5^{+1.1}_{-1.5}$ | $+0.23^{+0.05}_{-0.05}$ | 0.07 | $10.8^{+0.5}_{-0.6}$ | $+0.27^{+0.02}_{-0.02}$ | 0.76 |
| 4387 | $10.8^{+1.6}_{-2.3}$ | $-0.03^{+0.14}_{-0.10}$ | 0.39 | $10.2^{+1.3}_{-1.9}$ | $+0.01^{+0.12}_{-0.12}$ | 0.60 | $10.1^{+2.0}_{-2.4}$ | $-0.01^{+0.15}_{-0.12}$ | 0.66 | $10.1^{+1.1}_{-1.5}$ | $+0.18^{+0.05}_{-0.05}$ | 0.67 |
| 4458 | $10.3^{+1.7}_{-2.5}$ | $-0.22^{+0.12}_{-0.07}$ | 0.44 | $9.9^{+1.3}_{-2.2}$ | $-0.20^{+0.12}_{-0.07}$ | 0.50 | $9.9^{+1.9}_{-2.8}$ | $-0.19^{+0.17}_{-0.09}$ | 0.55 | $9.9^{+1.4}_{-2.0}$ | $+0.03^{+0.09}_{-0.08}$ | 0.13 |
| 4464 | $11.3^{+1.3}_{-2.3}$ | $-0.15^{+0.10}_{-0.10}$ | 0.64 | $10.4^{+1.2}_{-2.0}$ | $-0.12^{+0.13}_{-0.09}$ | 1.03 | $10.5^{+1.8}_{-2.6}$ | $-0.14^{+0.18}_{-0.11}$ | 1.07 | $10.3^{+1.1}_{-1.6}$ | $+0.10^{+0.06}_{-0.07}$ | 0.48 |
| 4467 | $6.5^{+2.7}_{-1.8}$ | $+0.07^{+0.11}_{-0.16}$ | 1.25 | $7.1^{+2.4}_{-1.9}$ | $+0.07^{+0.11}_{-0.15}$ | 1.40 | $7.5^{+2.8}_{-2.3}$ | $+0.14^{+0.11}_{-0.15}$ | 1.88 | $8.6^{+1.9}_{-1.9}$ | $+0.17^{+0.07}_{-0.08}$ | 1.07 |
| 4472 | $8.7^{+2.6}_{-1.9}$ | $+0.21^{+0.06}_{-0.11}$ | 1.30 | $8.9^{+1.7}_{-1.8}$ | $+0.22^{+0.05}_{-0.09}$ | 1.22 | $9.7^{+2.0}_{-2.6}$ | $+0.22^{+0.05}_{-0.08}$ | 1.76 | $10.3^{+0.8}_{-0.9}$ | $+0.26^{+0.02}_{-0.03}$ | 1.24 |
| 4473 | $11.5^{+1.0}_{-1.4}$ | $+0.22^{+0.05}_{-0.07}$ | 0.18 | $10.9^{+0.8}_{-1.1}$ | $+0.23^{+0.05}_{-0.05}$ | 0.22 | $11.3^{+1.2}_{-1.5}$ | $+0.22^{+0.05}_{-0.07}$ | 0.30 | $10.8^{+0.5}_{-0.7}$ | $+0.26^{+0.02}_{-0.02}$ | 0.77 |
| 4478 | $9.2^{+2.4}_{-2.6}$ | $+0.14^{+0.11}_{-0.14}$ | 0.01 | $9.0^{+1.8}_{-2.3}$ | $+0.16^{+0.10}_{-0.12}$ | 0.01 | $9.3^{+2.1}_{-2.7}$ | $+0.19^{+0.07}_{-0.13}$ | 0.01 | $9.9^{+1.1}_{-1.3}$ | $+0.25^{+0.03}_{-0.05}$ | 0.05 |
| 4489 | $4.3^{+1.7}_{-1.2}$ | $+0.06^{+0.13}_{-0.12}$ | 0.27 | $5.0^{+2.2}_{-1.6}$ | $+0.04^{+0.14}_{-0.12}$ | 0.31 | $6.4^{+2.4}_{-1.9}$ | $+0.11^{+0.13}_{-0.14}$ | 0.43 | $5.5^{+2.1}_{-1.2}$ | $+0.18^{+0.06}_{-0.08}$ | 0.52 |
| 4551 | $7.8^{+3.0}_{-2.0}$ | $+0.19^{+0.08}_{-0.14}$ | 0.59 | $8.1^{+2.1}_{-2.0}$ | $+0.20^{+0.07}_{-0.12}$ | 0.41 | $8.9^{+2.3}_{-2.8}$ | $+0.22^{+0.06}_{-0.11}$ | 0.73 | $9.6^{+1.0}_{-1.3}$ | $+0.25^{+0.03}_{-0.05}$ | 0.40 |
| 4621 | $11.5^{+1.0}_{-1.4}$ | $+0.23^{+0.05}_{-0.05}$ | 0.15 | $10.9^{+0.8}_{-1.1}$ | $+0.24^{+0.04}_{-0.04}$ | 0.19 | $11.3^{+1.1}_{-1.5}$ | $+0.23^{+0.05}_{-0.05}$ | 0.24 | $10.8^{+0.5}_{-0.6}$ | $+0.27^{+0.02}_{-0.02}$ | 0.65 |
| 4697 | $8.7^{+2.8}_{-2.1}$ | $+0.19^{+0.08}_{-0.14}$ | 0.89 | $8.7^{+2.0}_{-2.0}$ | $+0.20^{+0.07}_{-0.12}$ | 0.85 | $9.4^{+2.1}_{-2.6}$ | $+0.21^{+0.06}_{-0.12}$ | 1.30 | $10.1^{+0.9}_{-1.1}$ | $+0.25^{+0.02}_{-0.04}$ | 0.80 |

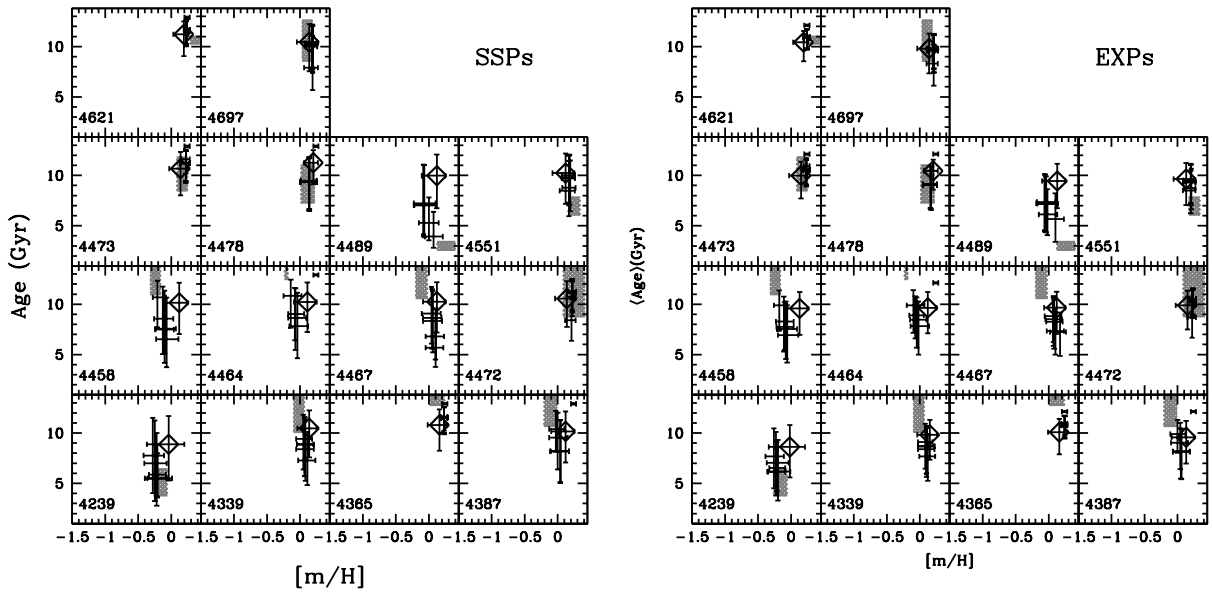


**Figure 6.** Best fit age and metallicity values for our sample, using SSPs (*left*) or EXP models (*right*). The error bars shown the 68% confidence levels and the shaded regions give the age and metallicity estimates of Yamada et al. (2006) using the H$\gamma_\sigma$ vs. [MgFe] diagram. The diamond gives the fit to the age and metallicity using *only* the spectral energy distribution (i.e. no line strengths are used for this data point).

either in the standard way or using the BMC pseudo-continuum. The shaded areas give to the difference in the EWs with respect to a reference stellar population: on the left it is the population with the same age at solar metallicity, and on the right the reference is a population with the same metallicity and 10 Gyr old, both references marked by the vertical lines. Black and grey shading correspond to the BMC and the side-band methods, respectively. The panels on the left explore the age-sensitive Balmer indices for a range of metallicities and the panels on the right show metal indices for a range of ages. Ideally, a perfect observable would result in a horizontal line (i.e. zero metallicity dependence of an age-sensitive line and vice-versa). The models span a wide range of ages and metallicities as shown in the caption. This figure shows that BMC-based measurements of EWs are less subject to the age-metallicity degeneracy than the side-band methods. This result is especially dramatic for H$\gamma$ and H$\delta$, for which the age-metallicity degeneracy drops from $\Delta\mathrm{EW}/\Delta\log(Z/Z_\odot) = -4.2$ (side-band) to $-1.9$ (BMC) in H$\gamma$ or from $-3.9$ (side-band) to $-1.7$ (BMC) in H$\delta$ (values measured at the fiducial 10 Gyr, solar metallicity SSP). Furthermore, the shaded regions of the metal-line indices on the rightmost panels are much wider for the BMC method (black), showing that at a fixed age, the BMC method spans a wider range of EW, thereby being more sensitive to metallicity (see caption for details).

Furthermore, we have compared the effect of noise on our proposed BMC pseudo-continuum and found that for a wide range of signal-to-noise ratios (from 10 to 100 per Å ) the uncertainty in the EW of all lines is always $\sim 0.3$ dex smaller than those obtained with the side-band method.

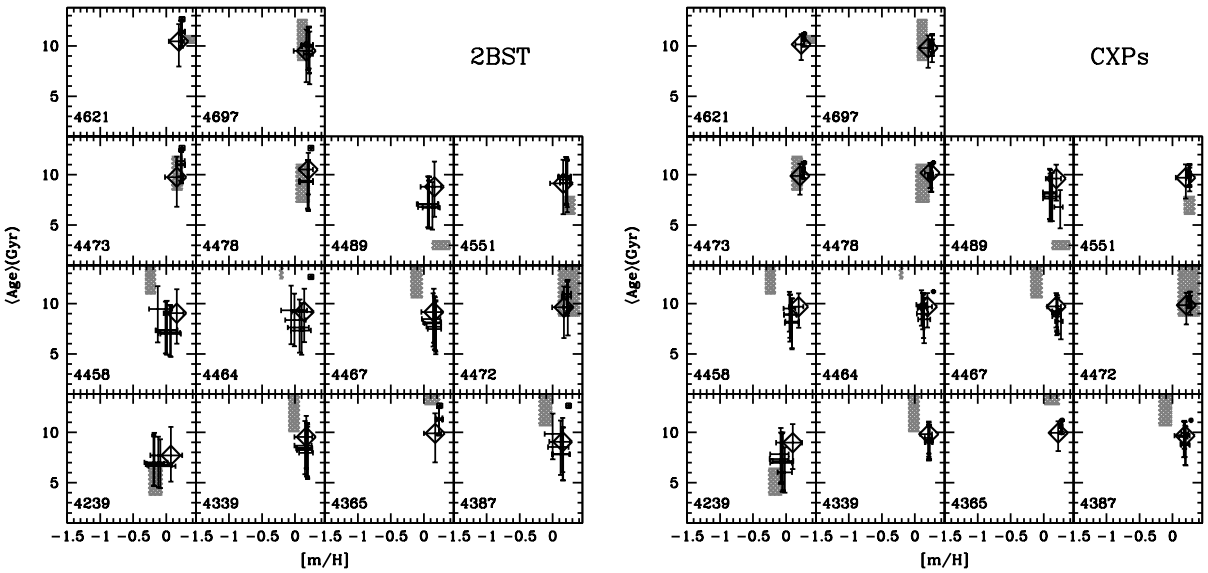


**Figure 7.** Best fit age and metallicity values for our sample, using 2-Burst (*left*) or CXP models (*right*). The error bars shown the 68% confidence levels and the shaded regions give the age and metallicity estimates of Yamada et al. (2006) using the H$\gamma_\sigma$ vs. [MgFe] diagram. The diamond gives the fit to the age and metallicity using *only* the spectral energy distribution (i.e. no line strengths are used for this data point).

Figure 5 shows the equivalent widths of several lines for a grid of SSPs corresponding to a velocity dispersion of 100 km/s (black) or 300 km/s (grey). The measured EWs (without any correction for velocity dispersion) are shown as black dots, along with a characteristic error bar which mostly comes from the systematics (the observed uncertainties are much smaller). We emphasize that our fitting method generates grids corresponding to the measured velocity dispersion for each galaxy. One can see that BMC EWs (left panels) appear less degenerate than the grids using a side-band method (right panels).

## 4 MODELLING THE SFH OF ELLIPTICAL GALAXIES

The properties of the unresolved stellar populations of our sample are constrained by comparing the targeted equivalent widths with four sets of generic models that describe the star formation history in terms of a reduced number of parameters. It is our goal to assess the consistency of different sets of models in fitting *independently* the different spectral lines targeted as well as the full SED. The majority of studies in the literature (see e.g. Kuntschner & Davies 1998; Trager et al. 2000; Caldwell et al. 2003; Thomas et al. 2005) have compared measurements of EWs with simple stellar populations (i.e. a single age and metallicity). While those models are probably valid for the populations found in globular clusters, it is imperative to go beyond simple stellar populations in galaxies, whose star formation histories generate complex distributions of age and metallicity. Ferreras & Yi (2004) and Pasquali et al. (2003) showed that composite models of stellar populations could result in significant differences on the average ages and metallicities of galaxies. More recently, Sánchez-Blázquez et al. (2006) and Serra & Trager (2007) have explored this issue through the comparison of two age indicators, both concluding that composite populations are needed to consistently model the populations in early-type galaxies.

In this paper, except for the first case (namely Simple Stellar Populations), the models generate a distribution of ages and/or metallicities that are used to combine the population synthesis models of Bruzual & Charlot (2003), assuming a Chabrier (2003) Initial Mass Function. The resulting synthetic spectral energy distribution is smoothed to the same resolution and velocity dispersion of the galaxy. A correction for Galactic reddening is applied, assuming the Fitzpatrick (1999) law (this is mostly done for the comparison of the full SEDs, as EWs are not affected). Finally, the EWs are computed and compared with the observations using a standard likelihood method. We sum in quadrature the uncertainties of the observed EWs (as given in table 1) with the systematic errors expected in the lines, as given in table 5 of Bruzual & Charlot (2003). The high S/N of the observed spectra imply that our error budget is mainly dominated by the systematics of the population synthesis models.

The four sets of models considered in this paper are listed below, with the range of parameters shown in table 2.

(i) Simple Stellar Populations (SSP): This has been the most popular method used in the analysis of the ages and metallicities of early-type galaxies. The advantage lies in it simplicity: SSPs are the building blocks of all population synthesis models, and they are carefully calibrated against realistic SSPs (i.e. globular clusters). An SSP is uniquely defined by an age and a metallicity. The drawback of this method is that the ages obtained are inherently *luminosity weighted*, such that a small amount of young stars can have a significant effect on the age extracted with this method. Furthermore, SSPs are not expected to model galaxy populations, which have an extended range of ages and metallicities. By using SSPs to model early-type galaxies one makes the assumption that the stellar populations have a narrow age distribution compared to stellar evolution timescales.

(ii) Exponential SFH (EXP): A more physical scenario should consider an extended period of star formation. The EXP models (also called $\tau$ models in the literature) model the star formation

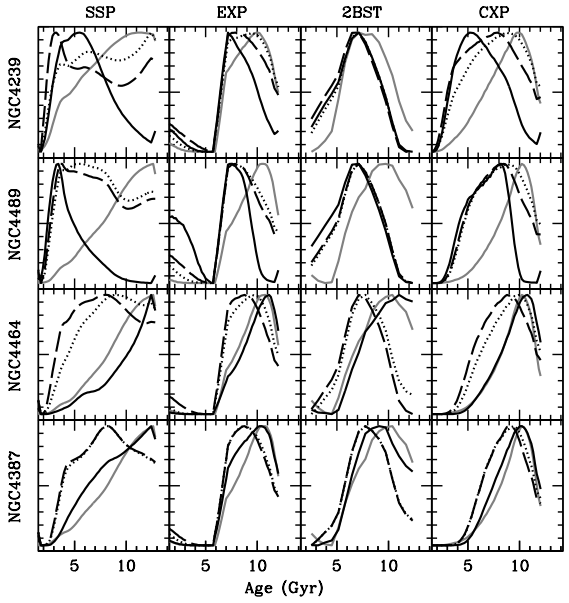


**Figure 8.** Likelihood distribution of the marginalised average stellar ages for some of the Virgo cluster elliptical galaxies from our sample. The distribution is shown for the four models as labelled. The grey solid line corresponds to the fit to the SED. The black lines lines correspond to the age distribution according to [MgFe] plus either H$\beta$ (solid), H$\gamma$ (dashed), or H$\delta$ (dotted), respectively.

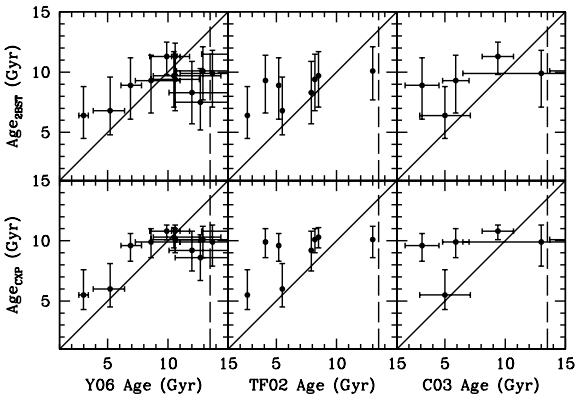


**Figure 9.** Comparison between the ages presented here and those from previous studies. Y06, TF02 and C03 indicate (Yamada et al. 2006), (Terlevich & Forbes 2002), and (Caldwell et al. 2003), respectively. The slanted solid line is a 1:1 correspondence. The vertical dashed line represents the age of the Universe for our cosmology, and is used as a prior in the analysis (see text for details).

rate as an exponentially decaying function of time with timescale $\tau$, started at an epoch given by a formation redshift $z_F$. The metallicity is assumed to be fixed throughout the SFH and is also left as a free parameter.

(iii) Two Burst Formation (2BST): Recent rest-frame NUV observations have revealed the presence of residual star formation in early-type galaxies (see e.g. Trager et al. 2000; Ferreras & Silk 2000; Yi et al. 2005; Kaviraj et al. 2007a). The presence of small amounts of young stars can significantly affect the derived SSP model parameters (Serra & Trager 2007). This model describes this mechanism with two simple stellar populations. Four parameters are left free: the age of the old ($t_O$) and the young components ($t_Y$), the mass fraction in young stars ($f_Y$), and the metallicity of the populations ($Z$, assumed to be the same for the old and the young components).

(iv) Chemically Enriched Exponential (CXP): All the models considered above fix the metallicity throughout the SFH. More realistically, a model should incorporate in a consistent way the buildup of metallicity caused by previous generations of stars. These chemical enrichment models (see e.g. Boissier & Prantzos 1999; Ferreras & Silk 2003) include the stellar yields from intermediate and massive stars and result in a distribution of metallicities as well as ages. The aim of this paper is to explore simple models that can be easily implemented. Hence, instead of applying a detailed model of chemical enrichment, we define in a purely phenomenological way a model that mimics those. We keep the same SFH as in the EXP models (described by a star formation timescale $\tau_1$ and a formation redshift $z_F$). Furthermore, the metallicity is assumed to increase in step with the cumulative distribution of the star formation rate, namely:

$$Z(t) = Z_1 + Z_2\Big[1 - \exp(\Delta t/\tau_2)\Big], \qquad (2)$$

where $\Delta t = t - t(z_F)$ and $\tau_2$ is the timescale corresponding to the buildup of metallicity. As a first-order approach it is valid to assume that metallicity increases with the stellar mass of the system (roughly, the cumulative distribution of the star formation rate). More accurately, this timescale will depend on the star formation efficiency or on the fraction of gas ejected in outflows (see e.g. Ferreras & Silk 2003). The upper and lower values of metallicity are fixed to $Z_1 = Z_\odot/10$ and $Z_2 = 2Z_\odot$, although the average metallicity will be controlled by the timescale $\tau_2$.

We assume a standard $\Lambda$CDM cosmology ($\Omega_m$=0.3; $H_0$= 70 km/s/Mpc) to constrain the maximum ages of the stellar populations to the age of the Universe (13.7 Gyr). One could allow the fitting algorithm to stray into older ages to explore wider volumes of parameter space, but this paper takes the cosmological constraints on the age of the Universe at face value (Spergel et al. 2007). Furthermore, population synthesis models are poorly calibrated for populations older than Galactic globular clusters. We note that previous work on the same spectra (Yamada et al. 2006) probed the population synthesis models of Vazdekis & Arimoto (1999) all the way to their oldest available ages (20 Gyr).

### 4.1 Disentangling the stellar populations

The comparison of the EWs is done by measuring the line strengths directly from the model SEDs after being resampled and smoothed to the resolution and velocity dispersion of the actual observations of each galaxy, taken from Yamada et al. (2006). Since the spectra of the models have already been smoothed in terms of velocity dispersion to that of the real galaxy, no correction for this need be applied. All galaxies are fitted using the age-sensitive indices, H$\beta_{20}$, H$\gamma_{20}$, H$\delta_{20}$, D4000 and G4300$_{20}$ along with the metallicity indicator [MgFe]$_{20}$(González 1993). This is used instead of the newer [MgFe]$'$ as defined by Thomas et al. (2003) since the original is almost independent of $\alpha$/Fe and it is not clear whether the same fractions of the two Fe lines is still appropriate for the new BMC indices.

As indicated by Schiavon et al. (2004) and later confirmed by Serra & Trager (2007), a discrepancy found between the parame-

**Table 4.** Best fit parameters for the 2BST and CXP models

| Galaxy | $M_s^1$ | 2BST | | CXP | | |
|---|---|---|---|---|---|---|
| NGC | $10^{10}M_\odot$ | $t_Y$(Gyr) | $f_Y$ | $\tau_1$(Gyr) | $\tau_2$(Gyr) | $z_F$ |
| 4239 | 0.9 | $2.3^{+0.3}_{-0.6}$ | $0.13^{+0.17}_{-0.11}$ | $0.3^{+0.8}_{-0.2}$ | $0.4^{+1.4}_{-0.3}$ | $0.8^{+0.7}_{-0.3}$ |
| 4339 | 4.3 | $2.2^{+0.4}_{-1.0}$ | $0.04^{+0.11}_{-0.04}$ | $0.6^{+0.6}_{-0.3}$ | $0.1^{+0.2}_{-0.1}$ | $1.9^{+1.5}_{-0.7}$ |
| 4365 | 39.5 | $1.4^{+1.0}_{-1.0}$ | $\lesssim 0.02$ | $0.9^{+0.3}_{-0.3}$ | $1.4^{+1.0}_{-1.0}$ | $4.1^{+0.8}_{-1.1}$ |
| 4387 | 2.8 | $1.6^{+0.9}_{-1.1}$ | $\lesssim 0.02$ | $0.5^{+0.4}_{-0.3}$ | $0.1^{+0.2}_{-0.0}$ | $2.5^{+1.6}_{-0.9}$ |
| 4458 | 2.0 | $2.0^{+0.6}_{-1.3}$ | $\lesssim 0.06$ | $0.3^{+0.5}_{-0.2}$ | $0.2^{+0.6}_{-0.1}$ | $2.2^{+1.6}_{-0.9}$ |
| 4464 | 1.4 | $1.6^{+0.9}_{-1.2}$ | $\lesssim 0.03$ | $0.3^{+0.5}_{-0.2}$ | $0.2^{+0.4}_{-0.1}$ | $2.5^{+1.6}_{-1.0}$ |
| 4467 | 0.3 | $2.3^{+0.4}_{-0.7}$ | $0.08^{+0.15}_{-0.08}$ | $0.5^{+0.8}_{-0.4}$ | $0.1^{+0.3}_{-0.1}$ | $1.6^{+1.5}_{-0.7}$ |
| 4472 | 66.5 | $2.0^{+0.6}_{-1.3}$ | $\lesssim 0.05$ | $0.9^{+0.5}_{-0.4}$ | $0.3^{+0.2}_{-0.2}$ | $3.2^{+1.3}_{-1.0}$ |
| 4473 | 22.4 | $1.5^{+1.0}_{-1.1}$ | $\lesssim 0.02$ | $0.9^{+0.3}_{-0.3}$ | $0.9^{+0.6}_{-0.6}$ | $4.1^{+0.9}_{-1.2}$ |
| 4478 | 4.2 | $2.0^{+0.6}_{-1.3}$ | $\lesssim 0.07$ | $0.8^{+0.5}_{-0.4}$ | $0.2^{+0.1}_{-0.1}$ | $2.6^{+1.6}_{-0.9}$ |
| 4489 | 1.0 | $2.3^{+0.4}_{-0.5}$ | $0.21^{+0.17}_{-0.15}$ | $0.6^{+0.7}_{-0.3}$ | $0.1^{+0.4}_{-0.1}$ | $0.7^{+0.7}_{-0.2}$ |
| 4551 | 3.0 | $2.1^{+0.5}_{-0.9}$ | $0.03^{+0.08}_{-0.03}$ | $1.0^{+0.6}_{-0.5}$ | $0.2^{+0.1}_{-0.1}$ | $2.5^{+1.6}_{-0.9}$ |
| 4621 | 32.7 | $1.5^{+0.9}_{-1.1}$ | $\lesssim 0.02$ | $1.0^{+0.3}_{-0.3}$ | $1.4^{+1.0}_{-1.0}$ | $4.1^{+0.9}_{-1.2}$ |
| 4697 | 14.7 | $2.0^{+0.6}_{-1.3}$ | $\lesssim 0.06$ | $0.9^{+0.5}_{-0.4}$ | $0.2^{+0.2}_{-0.1}$ | $2.9^{+1.6}_{-1.0}$ |

[1] Stellar masses are computed from the best fit CXP models. No significant changes found among models. Estimated uncertainty $\Delta \log M_s \sim 0.3$ dex (mostly from the assumption about the IMF).

ters derived through each of the three Balmer lines could be explained by the existence of an underlying younger sub-population. Schiavon et al. (2004) explain that this may well be due to the dominance of the younger population at bluer wavelengths. However the mere fact that different indices would give different parameters, should suggest that the model being used has not captured all aspects of the true star formation history. Hence, in the analysis of EWs of our sample galaxies, we are not only looking to determine the age and metallicity but also estimating whether it is possible to *rule out a single population* to describe an early-type galaxy. This could be done through discrepencies between the three Balmer lines targeted here.

With the same aim, we further expand this analysis beyond the Balmer lines, to include $D4000$ and the G Band. We are looking to observe discrepancies that will indicate that the model being used is not suitable.

### 4.2 Spectral Fitting

As an alternative approach to targeted line strengths, we also consider the full spectral energy distribution to constrain the star formation history of our sample. In this paper we want to test the consistency between the constraints imposed by the line strengths and those from a full spectral fit.

We use a maximum likelihood method to fit the spectra, which is analysed over the spectral range between 3900Å and 4500Å (or 4000–4500Å for the six galaxies observed with WHT). The SEDs are normalised over the same range. The data span a much wider spectral range (out to 5500-5800Å). However, we have chosen a smaller range to avoid flux calibration errors, which could introduce important systematic changes in the predicted ages and metallicities. The spectral range chosen straddles the D4000 break, since this is a very sensitive indicator of the ages of the stellar populations.

### 4.3 Results

Figures 6 and 7 show the average age and metallicity for all four models explored in this paper. The error bars are shown at the 69% confidence level (i.e. like a $1\sigma$ level although our analysis does not assume a Gaussian distribution). For the SSPs the average age is trivially the age of the population. For the others, the average values are weighed by the stellar mass. Each error bar corresponds to the *individual fit* of an age-sensitive line (H$\beta$, H$\gamma$, H$\delta$, G4300 or D4000) plus the [MgFe] as metallicity indicator (i.e. each point comes from the analysis involving 2 indices). The diamond and its error bar correspond to the fit to the SED – no additional information from the line strengths is added to this likelihood. In grey, the shaded areas correspond to the ages from Yamada et al. (2006) (using the H$\gamma_\sigma$ – [MgFe] diagram on SSPs). One can see that SSPs (left panel of figure 6) shows the largest discrepancies between the ages and metallicities estimated using independently the different age-sensitive indices. This would imply that a joint likelihood putting all indices together would not be a consistent way of determining the ages of the populations. Nevertheless, as a comparison we show in table 3 the best fit of the average age and metallicity, combining all indices (but not the fit of the SED). Table 4 shows the best fit parameters for the 2BST and CXP models. The uncertaintes in both tables are given at the 90% confidence level. We show in table 3 the minimum value of the $\chi^2_r$ (reduced chi-square) for each of the models. Notice that these values are often rather small, a result of the conservative systematic errors taken from Bruzual & Charlot (2003). The table shows that SSPs cannot be ruled out purely on the basis of their goodness of fit, as all models give reasonable values of $\chi^2_r$. Nevertheless, the discrepancies among individual measurements shown in figure 6 reflects the fact that a single age and metallicity scenario is a weaker, less consistent model of the populations of a galaxy. Table 3 shows that the actual change in the age when going beyond SSPs can be quite significant, especially for younger ages. We emphasize here that the different ages do not reflect a possible inclusion of a prior caused by the choice of parameters. All the composite models presented here (CSP, EXP and 2-Burst) explore a range of parameters that includes the best-fit ages and metallicities obtained by the SSPs.

The mismatch discussed above can be seen in more detail in figure 8, where the marginalised distribution of average age for all four models is shown for a few galaxies from the sample, as labelled. The solid, dashed, and dotted lines correspond to individ-

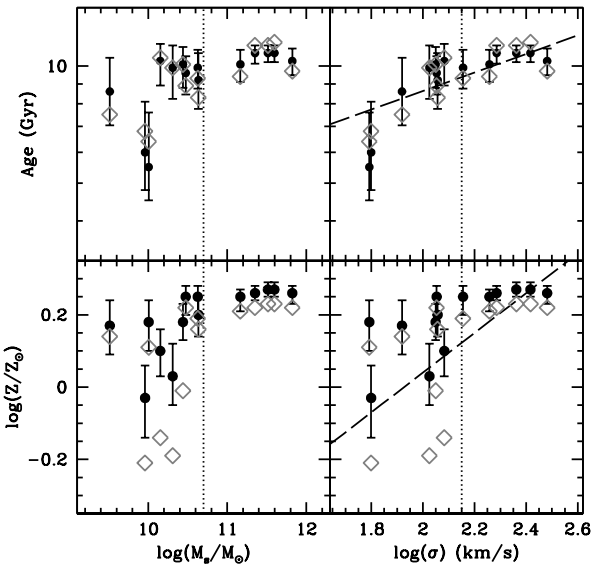


**Figure 10.** Ages and metallicities versus stellar mass (left) and velocity dispersion (right). The solid dots (grey diamonds) correspond to the estimates from the CXP (2-Burst) models. The dashed lines in the rightmost panels are the age and metallicity scaling relation of Thomas et al. (2005).

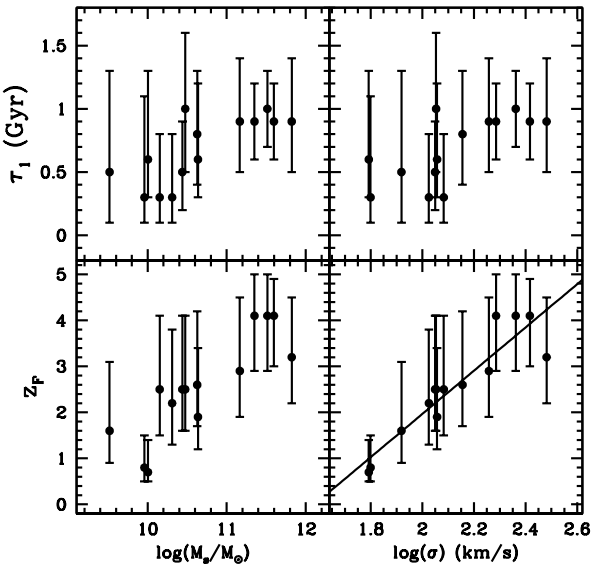


**Figure 11.** The predictions of the CXP models for star formation timescale (*top*) and formation redshift (*bottom*) are shown with respect to stellar mass (*left*) and velocity dispersion (*right*). This speculative plot suggests that the age trend found in figure 10 is caused by a range of formation epochs, rather than formation timescale, which is shown to be roughly independent of galaxy mass in the top panels. The solid line in the bottom right panel is a simple linear fit to the data (equation 3, see text for details).

ual fits to H$\beta$, H$\gamma$, and H$\delta$, respectively, along with the best fit only using the SED (grey line). SSPs (leftmost panels) fail to give a consistent distribution, whereas any of the other models give a more unified distribution. Notice that the galaxies shown in the top panels (NGC 4239 and NGC 4489) have young populations, whereas the bottom two galaxies (NGC 4464 and NGC4387) have overall older populations. The top two galaxies are better fit by a 2-Burst model and the bottom two get better fits from an extended model like CXP. This would suggest that the youngest populations in early-type galaxies are best fit by the assumption of "sprinkles" of young stars, as suggested by Trager et al. (2000) and modelled by Ferreras & Silk (2000) and Kaviraj et al. (2007a).

Figure 9 shows a comparison of our age estimates using 2-Burst (*top*) and CXP models (*bottom*) with values taken from the literature, as given in the figure caption. It is important to notice that our models do not consider ages older than the age of the Universe using a concordance $\Lambda$CDM cosmology (i.e. 13.7 Gyr). For the youngest galaxies, our analysis gives rather older ages than previous estimates from the literature. Figure 10 shows the average age and metallicity as a function of stellar mass (*left*) and velocity dispersion (*right*), both for the CXP (black dots) and for the 2-Burst models (grey diamonds). The stellar masses are obtained by combining the absolute magnitude of the galaxies in the $V$ band with $M/L_V$ corresponding to the best fit CXP models (There is no significant difference if the best fit 2-Burst models are used instead). The dashed line is the fit to age and metallicity from Thomas et al. (2005). Our age-mass relationship is compatible with recent estimates in the literature (see e.g. Trager et al. 2000; Caldwell et al. 2003; Thomas et al. 2005; Sánchez-Blázquez et al. 2006b). Notice that Sánchez-Blázquez et al. (2006b) find no correlation between age and mass at the higher densities of the Coma cluster. We should also emphasize that our reduced sample of Virgo *elliptical* galaxies excludes massive, young S0s in high density environments (Thomas et al. 2005), possibly the cause of the age scatter found by the other groups.

Notice in figure 10 the transition in the age distribution around 140 km/s in velocity dispersion or $5{\times}10^{10}M_{\odot}$ in stellar mass. Above this value the ages of the populations are overall old and with small scatter among galaxies, whereas lower mass galaxies have a wide range of ages and metallicities (not necessarily younger throughout). The trend is robustly independent of the modelling, as shown both by the CXP fits (black dots) and the 2-Burst models (grey diamonds). This threshold is reminiscent of the one found by Kauffmann et al. (2003) in the general population of SDSS galaxies at a stellar mass $3 \times 10^{10}M_{\odot}$ or the threshold in star formation efficiency of late-type galaxies at rotation velocities $v_c$ $\sim$140 km/s based on their photometry (Ferreras et al. 2004) or on the presence of dust lanes (Dalcanton et al. 2004).

## 5 CONCLUSIONS

We have revisited the superb, high signal-to-noise spectra of 14 elliptical galaxies in the Virgo cluster presented by Yamada et al. (2006, 2008). Our main goal was two-fold: a) to give an optimal but versatile definition of the equivalent width of spectral features that would minimise the contribution from nearby lines, b) to explore the possibility of discriminating between the standard treatment of galaxy spectra either as simple stellar populations or composite models with a distribution of ages and metallicities.

The former was achieved by defining a "boosted median" pseudo-continuum. This method is very easy to implement on any spectral data and it improves on the traditional side-band methods by reducing the final uncertainty of the EWs for the same spectra and reducing the age-metallicity degeneracy of age- and

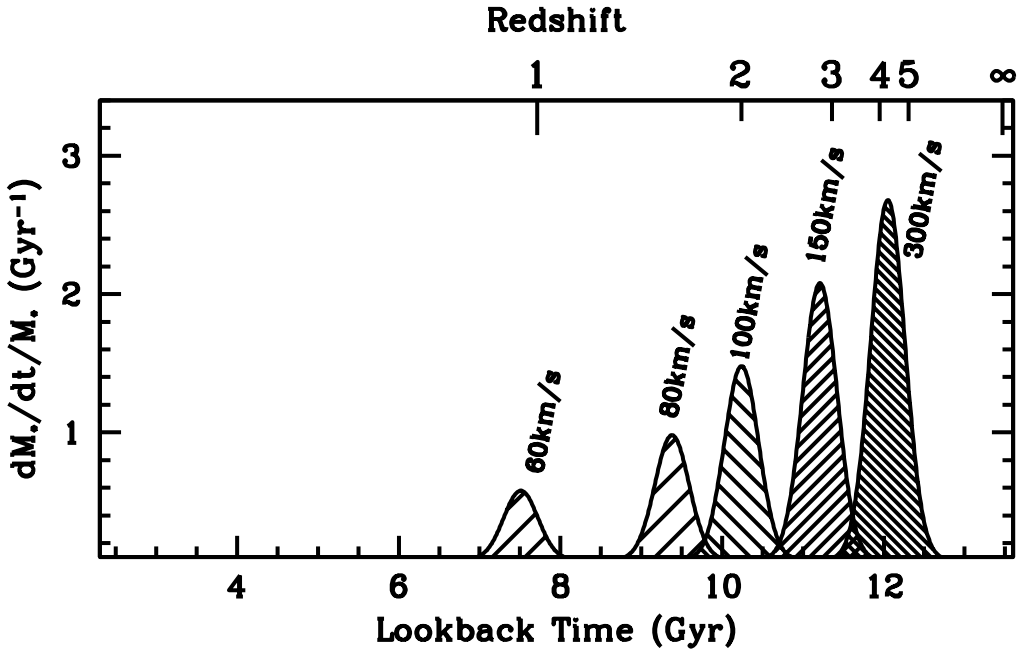


**Figure 12.** Our proposed model for the star formation history of Virgo cluster elliptical galaxies. The parameter estimates suggest a nearly constant star formation timescale with respect to velocity dispersion, whereas formation *epoch* is strongly correlated. We find a stronger correlation with velocity dispersion (compared to stellar mass), so we label the formation scenarios according to $\sigma$.

metal-sensitive lines by reducing the effect of unwanted, nearby spectral features. The method only requires two numbers to determine the pseudo-continuum (i.e. confidence level of the boosted median and size of the kernel over which the analysis is performed). We propose 90% and 100Å for these two parameters when dealing with stellar populations of galaxies at moderate resolution (R$\sim 1000-2000$).

The second goal – going beyond SSPs – is approached by comparing SSPs and three more sets of models which assume some distribution of ages and metallicities. We find simple populations fail to give a consistent marginalised distribution of ages when fitting independently different age-sensitive lines. We propose either a 2-Burst model or a $\tau$ star formatiom history with a phenomenological prescription for chemical enrichment (CSP models). They give similar results, with a clear trend between average age and either stellar mass or velocity dispersion, as shown in figure 10.

As suggested above when discussing figure 8, if younger (older) galaxies are better fit by 2-Burst (CXP) models, one would expect that young stars in ellipticalgalaxies appear in a random way, and not as a time-coherent, smooth distribution. This result supports minor merging – possibly involving metal-poor sub-systems – as the main mechanism to generate recent star formation in early-type galaxies (Kaviraj et al. 2007b). This process will be readily detected in low-mass galaxies, whereas a similar amount of young stars in a massive galaxy will be harder to detect.

Doubtlessly average ages and metallicities are the observables best constrained by these models. Parameters like formation timescale and formation epoch can only be considered "next-order" observables, which will be fraught with larger uncertainties. However, in a more speculative way, if we take the continuous CXP models at face value and put equal trust on the predictions of their formation epochs and timescales, figure 11 reveals an intriguing trend that suggests it is not formation timescale but formation *epoch* what drives the mass-age relationship in early-type galaxies. The solid line in the bottom-right panel gives a simple linear fit to the data, namely:

$$z_F \sim 2 + 4.7 \log \sigma_{100}, \quad (3)$$

with $\sigma_{100}$ given in units of 100 km/s. Figure 12 shows our proposed model for the star formation history of Virgo cluster elliptical galaxies. We model the formation histories as Gaussians with a similar spread (i.e. star formation timescale) with a correlation between formation epoch and velocity dispersion, as labelled.

One could argue that the lack of a correlation between formation timescale ($\tau_1$; *top*) and mass would contradict the observed relationship between mass and abundance ratios (see e.g. Thomas et al. 2005). One possibility would involve minor merging of dwarf galaxies. Those mergers will have a more prominent effect on the spectra of low-mass galaxies. Dwarf galaxies have a very extended period of star formation and eject a big fraction of their metals, resulting in metal-poor gas with solar or sub-solar abundance ratios that will reduce the observed (luminosity-weighted) [$\alpha$/Fe] in low-mass galaxies. Alternatively, notice that the formation epoch ($z_F$; *bottom*) correlates quite strongly with velocity dispersion, implying that the structures that form the bulk of the stars in low-mass galaxies are more likely to be contaminated by the ejecta from type Ia supernova, thereby reducing the abundance ratios to reproduce the observed correlation between [$\alpha$/Fe] and mass. A more detailed analysis of the abundance ratios – although beyond the scope of this paper – is under way to explore this very interesting possibility.

**ACKNOWLEDGEMENTS**

This work has made use of the delos computer cluster in the physics department at King's College London.

**REFERENCES**

Balogh, M. L., Morris, S. L., Yee, H. K. C., Carlberg, R. G., Ellingson, E., 1999, ApJ, 527, 54
Boissier, S., Prantzos, N., 1999, MNRAS, 307, 857
Bruzual, G., Charlot, S., 2003, MNRAS, 344, 1000
Caldwell, N., Rose, J. A., Concannon, K. D., 2003, AJ, 125, 2891
Chabrier, G., 2003, PASP, 115, 763
Dalcanton, J. J., Yoachim, P., Bernstein, R. A., 2004, ApJ, 608, 189
Ferreras, I., Silk, J., 2000, ApJ, 541, L37
Ferreras, I., Silk, J., 2003, MNRAS, 344, 455
Ferreras, I., Yi, S. K., 2004, MNRAS, 350, 1322
Ferreras, I., Silk, J., Böhm, A., Ziegler, B., 2004, MNRAS, 355, 64
Fitzpatrick, E. L., 1999 PASP, 111, 63
Gonzalez, J. J., 1993, Ph.D. thesis, Univ. California, Santa Cruz
Idiart, T. P., Silk, J., de Freitas Pacheco, J. A., 2007, MNRAS, 381, 1711
Jones, L. A., Worthey, G., 1995,ApJ, 446, L31
Kauffmann, G., et al., 2003, MNRAS, 341, 54
Kaviraj, S., et al., 2007a, ApJS, 173, 619
Kaviraj, S., Peirani, S., Khochfar, S., Silk, J., Kay, S., 2007b, arXiv:0711.1493
Kuntschner, H., Davies, R. L., 1998, MNRAS, 295, L29
McElroy, D. B., 1995, ApJS, 100, 105
Morelli, L, et al., 2004, MNRAS, 354, 753
Pasquali, A., Larsen, Søren, Ferreras, I., Gnedin, O. Y., Malhotra, S., Rhoads, J. E., Pirzkal, N., Walsh, J. R., 2005, AJ, 129, 148
Prochaska, L. C. et al., 2007, AJ, 134, 321
Rose, J. A., Bower, R. G., Caldwell, N., Ellis, R. S., Sharples, R. M., Teague, P., 1994, AJ, 108, 2054
Sánchez-Blázquez, P., Gorgas, J., Cardiel, N., González, J. J., 2006, A& A, 457, 787
Sánchez-Blázquez, P., Gorgas, J., Cardiel, N., González, J. J., 2006b, A& A, 457, 809
Schiavon, R. P., Caldwell, N., Rose, J. A., 2004, AJ, 127, 1513
Schlegel, D. J., Finkbeiner, D. P., Davis, M., 1998, ApJ, 500, 525
Serra, P., Trager, S. C., 2007, MNRAS, 374, 769
Spergel, D. N., et al., 2007, ApJS, 170, 377
Terlevich, A. I., Forbes, D. A., 2002, MNRAS, 30, 547
Thomas, D., Maraston, C., Bender, R., 2003, MNRAS, 339, 897
Thomas, D., Maraston, C., Korn, A., 2004, MNRAS, 351, L19
Thomas, D., Maraston, C., Bender, R., Mendes de Oliveira, C., 2005, ApJ, 621, 673
Trager, S. C., Faber, S. M., Worthey, G. , Gonzlez, J. J, 2000, AJ, 120, 165
Vazdekis, A. , Arimoto, N., 1999, 525, 144
Worthey, G., Faber, S. M., Gonzalez, J. J., Burstein, D., 1994, ApJS, 94, 687
Worthey, G., 1994, ApJS, 95, 107
Worthey, G., Ottaviani, D.L., 1997, ApJ, 111, 377
Yamada, Y., Arimoto, N., Vazdekis, A. , Peletier, R. F., 2006, ApJ, 637, 200
Yamada, Y., Arimoto, N., Vazdekis, A., Peletier, R. F., 2008, ApJ, 674, 612
Yi, S. K., et al., 2005, ApJ, 619, 111